Investigation of Striation Formation in Thin Stainless Steel Tube during Pulsed Nd:YAG Laser Cutting Process by Numerical Simulation

BYOUNG-CHEOL KIM, TO-HOON KIM, YANGSOO JANG, and KWANG-HOE CHUNG

The formation of a striation pattern in a thin stainless steel tube was investigated by numerical simulation during a pulsed Nd:YAG laser cutting process. The simulated results were compared with the experimental results, which were performed under the same conditions for simulation. The simulated results showed good agreement with the experimental results. Although the formation of the striation pattern was influenced by various laser parameters, the laser power density had become the most important factor in the formation of striation patterns, since the laser power density is the most influential in the heating of metal, and the striation formation is caused by the ejection of molten metal and evaporation during laser cutting process. Although a high power density resulted in clear regular striation patterns, relatively low power density caused the formation of a hot spot, which hindered the formation of regular striation patterns and caused less striation. The numerical simulation calculations can be used to predict the shape of striation patterns and to offer a way to provide a smooth cut wall.

I. INTRODUCTION

LASER cutting is widely used as a method of cutting various materials, because it renders a narrow kerf width, a high material removal rate and high dimensional accuracy. The laser cutting process is frequently adapted to high precision cutting of thin metal sheet and scribing of ceramics due to the small beam spot size and automatic control technology. Recently, precision laser cutting has been widely applied for electronic components and medical devices, and its applications are continuously growing.

Generally, laser cutting of metal sheet develops a periodic striation pattern, which affects the quality of the finished cut surface. The control of striation formation is very important in laser cutting of precision components in comparison with conventional cutting methods due to the limitation of post-treatment. Many studies have been done to investigate striation formation, and several mechanisms have been proposed.[1] It was known that the striation patterns formed by a continuous laser beam were primarily due to the oscillating molten front, which was affected by absorbance of the laser beam and interaction with the gas flow. However, the mechanism of striation formation is not clear and is not fully understood. Bunting and Cornfield[2] suggested a practical model of laser cutting, and Duley[3] determined cutting quality by considering evaporation and melt ejection. Arata *et al.*[4] conducted experimental work and suggested that the ignition and extinction cycles of the reaction began to take place below a certain cutting speed. Ivarson *et al.*[5] developed a cyclic oxidation model in which the oxidation rate was rapid in the early stage but decreased as the oxide layer thickness was increased. Once the oxide layer was blown out from the cutting front, the oxidation rate increased again. Striation formation was mostly discussed for continuous laser beam cutting, but that induced by a pulsed laser beam was not well developed. Laser cutting is definitely thermal processing, and thus it can be assumed that the striation formation induced by pulsed laser beam is similar to that by a continuous laser beam. However, the mechanism will be more complex in a pulsed laser beam than by a continuous laser beam.

When a pulsed laser beam is irradiated on a metal surface, the work piece has a different thermal distribution both in depth and lateral direction with time due to many variables such as laser beam absorbance, pulse width, beam frequency, and scanning speed. Also, this implies that the oxidation is varied with time and location. If the temperature reaches the melting point on the specimen, laser beam absorbance increases suddenly, and the melting and oxidation of the focused region is accelerated. At the same time, molten metal is ejected and the solid metal surface underneath is exposed to the laser beam. The temperature of the newly exposed surface will be higher than that of the initially irradiated surface, because of prior heating by molten metal and oxidation. Therefore, the new surface reaches the melting point quickly. However, if the laser beam is terminated, the temperature will drop quickly. In a pulsed laser beam cutting process, the cycle of a relatively short heating period and a relatively long cooling period is repeated and the temperature of the cutting front will change quickly. Although the striation formation is affected by the gas flow rate, properties of the molten layer, and oxygen diffusion through the oxide layer, the laser beam energy input on the surface will determine the striation patterns and oxidation ignition in the pulsed laser cutting process. It was reported that the oxidation heat contributed over 30 pct of the total heat input in the laser cutting process.[6] The oxidation will affect the quality of the cut wall, and irregular heat generation by oxidation will affect the striation formation in the laser

BYOUNG-CHEOL KIM, Graduate Student, and TO-HOON KIM, Professor, Department of Materials Science and Engineering, YANGSOO JANG, Professor, College of Medicine, and KWANG-HOE CHUNG, Professor, Department of Biochemistry, College of Science and Bioproducts Research Center, are with Yonsei University, Seoul 120-749, Korea.

Manuscript submitted November 13, 2000.

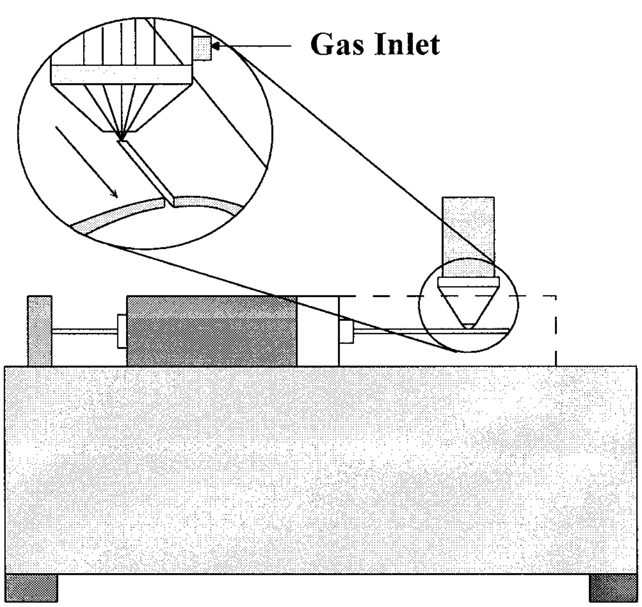

Fig. 1—Schematic diagram of laser cutting mechanism.

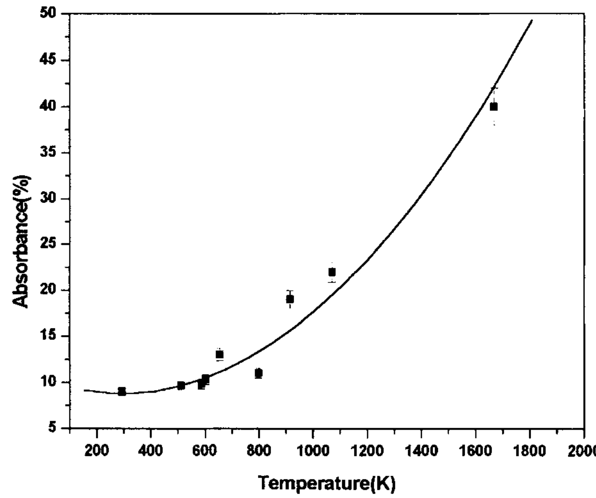

Fig. 2—Laser beam absorbance as a function of temperature obtained by numerical simulation for STS 304 stainless steel.[8]

cutting process. Many researchers have conducted heat transfer analyses of laser material processing. Mazumder and Steen[7] had applied Finite Differential Method (FDM) in a laser welding process, and an FDM- or Finite Element Method (FEM)-based heat transfer equation had been adopted as a useful tool for laser material processing.

In the present study, the formation of a striation pattern in a thin stainless steel tube was investigated during a pulsed Nd:YAG laser cutting process by numerical simulation. For this purpose, heat transfer analysis and striation formation have been conducted by FDM on the assumption that the most important cause of striation formation is the irregular heat generation in the cutting front, which was induced by the heat conduction situation and the related laser beam cutting parameters. The simulation was conducted for the cutting of a thin STS 316L stainless steel tube by the pulsed Nd:YAG laser beam with an oxygen-assisted gas. The temperature distribution was simulated under a transient three-dimensional condition, and the calculated results were compared with experimental results.

II. THEORETICAL BACKGROUND

A. *Physical Model*

A physical diagram of the reaction gas-assisted laser cutting is shown in Figure 1. A pulsed Nd:YAG laser beam was focused on the surface of a thin tube, and this tube was moved at a constant speed. The laser beam energy and oxidation energy heated the specimen, and gas flow expelled the molten metal from the cutting front. As the specimen temperature was increased from room temperature to the melting temperature, the laser beam absorbance increased, because the laser beam absorbance on the metal surface was a function of temperature. Laser beam absorbance on STS 304 stainless steel was calculated as a function of temperature by numerical analysis,[8] as shown in Figure 2. As shown in this figure, laser beam absorbance reached about 50 pct at the melting point. It is a well-known fact that the laser beam absorbance is a function of surface temperature and surface roughness. As the temperature of metal reaches the melting point, the metal phase is no longer a crystal structure but an amorphous phase. Then, the laser beam absorbance increases drastically. Also, the melted surface is no longer flat due to fluctuations by surface evaporation and shielding gas blowing. Thus, it can be assumed to be about 50 pct at the melting point. As the wavelength of the laser beam decreases, the laser absorbance increases on the metal surface. Thus, the absorbance of the Nd:YAG laser beam is higher than that of the CO_2 laser beam. However, the absorbance of the Nd:YAG laser beam as a function of temperature on stainless steel is not available. And, if the metal is melted, the laser beam absorbance increases drastically to a high value regardless of laser wavelength. Therefore, the available CO_2 absorbance was used in this work. Although there was a lack of high-temperature data and results were obtained with a CO_2 laser beam on STS 304 stainless steel, extrapolation of these data has been used in this work. Although laser absorbance was obtained for STS 304 stainless steel, it can be assumed that there is not any big difference for STS 316 stainless steel, since the composition of STS 316 stainless steel is not much different from STS 304 stainless steel except about 2 pct Mo in steel. The thermal conductivity and specific heat of the metal are functions of temperature. In the calculation of temperature distribution by FDM simulation in this work, the material properties such as thermal conductivity and specific heat used were those of STS 304L stainless steel, and their temperature dependencies were considered in the computer simulation. Also, the latent heat of melting and freezing was considered in the computer simulation by the temperature recovery method.[9]

The oxidation exothermic energy was taken into account during the laser cutting process. Although it was known that the oxidation energy contributed about 40 pct[6] of the total energy to the cutting process, this was not clearly proposed for the oxidation rate with temperature and the reaction temperature. Therefore, this simulated calculation assumed that the oxidation energy was generated at just above the melting point (2000 K) at once, and 30 pct of the total energy was contributed by this oxidation energy in the cutting process. Because STS 316L stainless steel contains Fe(68 pct), Cr(18 pct), and Ni(14 pct), the reaction heat energy took into account those values for Fe_2O_3, Cr_2O_3, and NiO, as shown subsequently:

(a) $2Fe + 3/2O_2 \rightarrow Fe_2O_3$, $\Delta H = -826.72$kJ/mol at 2000 K;
(b) $2Cr + 3/2O_2 \rightarrow Cr_2O_3$, $\Delta H = -1163.67$kJ/mol at 2000 K; and
(c) $Ni + 1/2O_2 \rightarrow NiO$, $\Delta H = -248.23$kJ/mol at 2000 K.

Although the laser beam density might be high enough to exceed the boiling point on a local area, it was assumed that the average energy density was not sufficient to form a keyhole only by evaporation in this cutting process. Thus, the temperature of the matrix was less than the boiling point, and excess energy over the boiling point was converted to mass removal. In the computer simulation calculation, the size of the model tube was 0.5 mm in length, 0.125 mm in thickness, and 1.8 mm in outer diameter, and the mesh number of elements was about 100,000. One element size was approximately 5×5 μm and the focused laser beam spot size was about 15×15 μm. Thus, one spot size area involved nine mesh elements. The smaller mesh size gives rise to more calculations and involves difficulties of convergence. Therefore, the mesh size was optimized through the simulated calculation. The preceding assumptions were summarized as follows, and they were considered in the simulated computer calculation.

(1) The laser beam absorbance, thermal conductivity, and specific heat were dependent upon the temperature of the specimen and the density of the specimen was constant.
(2) The effect of plasma was not considered, and the radiation heat loss was neglected, because it was much smaller than the melt ejection heat loss.
(3) The oxidation energy of the material was taken into account at 2000 K, and it contributed 30 pct of the total heat in each element.
(4) The melt temperature was sustained below the evaporation point, and the evaporation heat loss was taken into account for the mass removal.

B. *Governing Equation and Boundary Condition*

The simulation was conducted by a three-dimensional transient problem. Although the specimen was tube shaped, the dimension of the diameter was much larger than the thickness, and the laser spot size was much smaller than the thickness of the tube. Thus, it could be assumed that the tube became a sheet when the tube was spread flat, and the partial differential equation for heat transfer is given in Eq. [1].

$$\rho C_p\left(\frac{dT}{dt}\right) = \frac{d}{dx}\left(\mathrm{k}\frac{dT}{dx}\right) + \frac{d}{dy}\left(\mathrm{k}\frac{dT}{dy}\right) + \frac{d}{dz}\left(\mathrm{k}\frac{dT}{dz}\right) + Q_s \qquad [1]$$

In order to overcome geometric difficulties and to generalize numerical simulation, the control volume method was used to solve the partial differential equation for heat transfer. Figure 3 shows the nomenclature of the control volume approach and a mesh divided by an outer nodal point method, which was convenient for the boundary problem. The generalized equation from the control volume method, which adopted the Crank–Nicolson method, is given by Eq. [2].

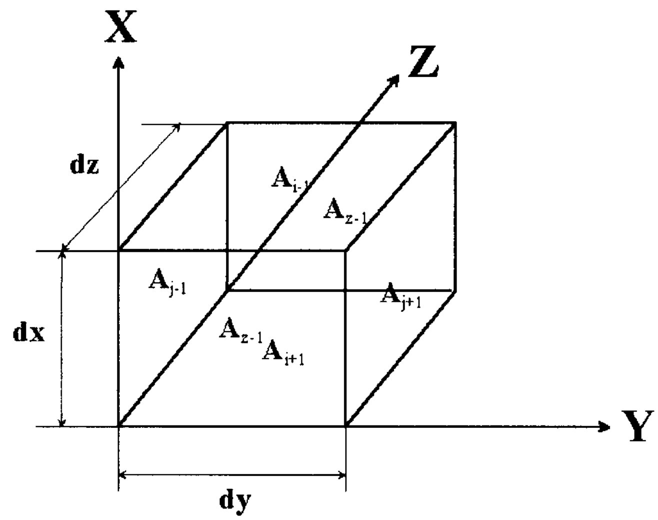

Fig. 3—Schematic drawing of nodal point in control volume method.

$$\begin{aligned} T^{t+dt}_{i,j,k} = T^t_{i,j,k} + \left(\frac{dt}{\rho \mathrm{C}_p V_{i,j,k}}\right)&(B_{i-1,j,k}A_{i-1,j,k}(T^{t+dt}_{i-1,j,k} - T^i_{i,j,k}) \\ &+ B_{i-1,j,k}A_{i-1,j,k}(T^t_{i-1,j,k} - T^t_{i,j,k}) \\ &+ B_{i+1,j,k}A_{i+1,j,k}(T^{t+dt}_{i+1,j,k} - T^t_{i,j,k}) \\ &+ B_{i+1,j,k}A_{i+1,j,k}(T^t_{i+1,j,k} - T^t_{i,j,k}) \\ &+ B_{i,j-1,k}A_{i,j-1,k}(T^{t+dt}_{i,j-1,k} - T^t_{i,j,k}) \\ &+ B_{i,j-1,k}A_{i,j-1,k}(T^t_{i,j-1,k} - T^t_{i,j,k}) \\ &+ B_{i,j+1,k}A_{i,j+1,k}(T^{t+dt}_{i,j+1,k} - T^t_{i,j,k}) \\ &+ B_{i,j+1,k}A_{i,j+1,k}(T^t_{i,j+1,k} - T^t_{i,j,k}) \\ &+ B_{i,j,k-1}A_{i,j,k-1}(T^{t+dt}_{i,j,k-1} - T^t_{i,j,k}) \\ &+ B_{i,j,k-1}A_{i,j,k-1}(T^t_{i,j,k-1} - T^t_{i,j,k}) \\ &+ B_{i,j,k+1}A_{i,j,k+1}(T^{t+dt}_{i,j,k+1} - T^t_{i,j,k}) \\ &+ B_{i,j,k+1}A_{i,j,k+1}(T^t_{i,j,k+1} - T^t_{i,j,k})) \end{aligned} \qquad [2]$$

Where

ρ = density;
C_p = specific heat;
$B_{i,j,k}$ = thermal resistant coefficient of elements of i, j, and k; and $A_{i,j,k}$ = area of $A_{i,j,k}$.

The initial condition was defined as that when the temperature of the specimen was 293 K at the initial state, as in Eq. [3].

$$T = T_0(x, y, z) \quad \text{at } t = 0 \qquad [3]$$

The convective heat transfer was considered in the boundary, and the convective heat transfer coefficient h_c was required for solving Eq. [2]. The convective heat transfer coefficient was obtained by Eq. [4].[10]

$$h_c = (k_g \cdot \mathrm{Nu}_m)/D \qquad [4]$$

where Nu_m is the Nusselt number, K_g is the thermal conductivity of air, and D length of element

The Nusselt number was defined by Eq. [5][10]

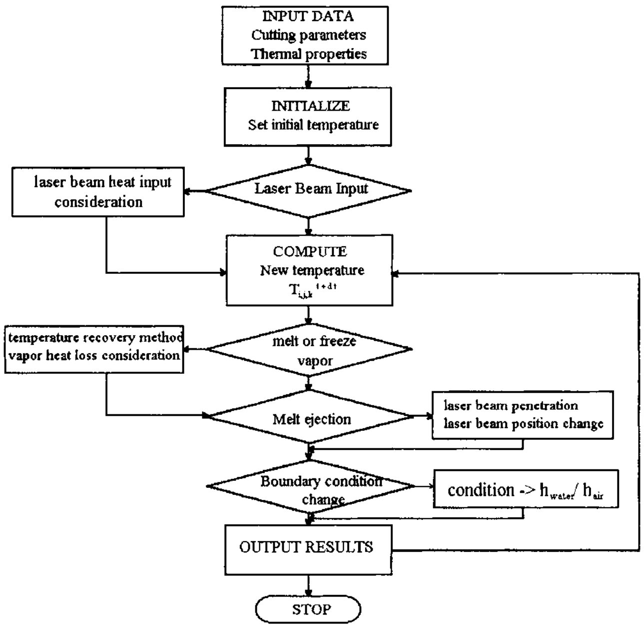

Fig. 4—Simplified flow chart of computer program.

$$\mathrm{Nu}_m = 0.3 + \frac{0.62\mathrm{Re}^{1.2}\mathrm{Pr}^{1/3}}{[1 + (0.4/\mathrm{Pr}^{2/3})]^{1/4}} \left[1 + \left(\frac{\mathrm{Re}}{282{,}000} \right)^{5/8} \right]^{4/5} \quad [5]$$

where *Re* is the Reynolds number and *Pr* is the Prandtle number.

The calculated convective coefficient was different between the inner surface and the outer surface, because enforced cooling was carried out with a cooling medium inside the tube in the experiment. If the element had a free surface, melt ejection occurred in the molten state. If melt ejection occurred, the boundary condition had changed from conduction to convection in the reference element until the next calculation step. The fixed temperature of the molten element was assumed to be sustained, and the laser beam was irradiated on the next element below the molten element, which was ejected.

Equation [2] provided large algebraic calculations and was solved by the Gauss–Seidal method, which was a kind of iteration method. In order to converge the algebraic equation and to provide enough time to satisfy the melt ejection effect, the time-step was defined to be as small a value as possible. The simplified flow diagram for computer calculation is illustrated in Figure 4.

III. EXPERIMENTAL PROCEDURES

In order to compare the simulated results with experimental results, the experiments were performed with a pulsed Nd:YAG laser. The beam mode was modulated to a Gaussian mode by a pinhole. The power used in this work was below 5.5 W, and the focused beam spot size was 15 μm in diameter. The throat diameter of the nozzle used for cutting was 1 mm, and the oxygen-assisted gas pressure was kept constant at 4 bar. The specimen was a STS 316L stainless steel tube with a thickness of 0.125 mm, a diameter of 1.8 mm, and a surface roughness of 1.0 μm root-mean-square.

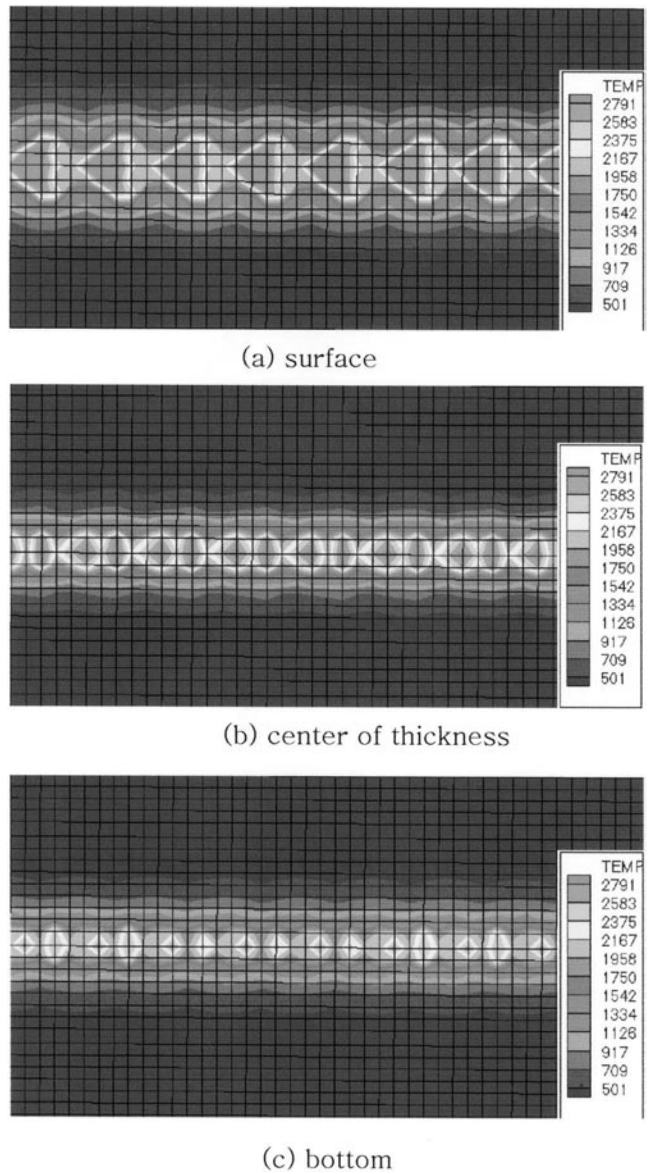

Fig. 5—Simulated temperature distributions in stainless steel tube by a pulsed Nd:YAG laser with 3.9 W of power, pulse duration of 0.12 ms, frequency of 600 Hz, and scanning speed of 300 mm/min. Each mesh size was 5 μm: (*a*) surface, (*b*) center of thickness, and (*c*) bottom.

The tube was moved at constant speed in the axial direction during laser irradiation, as shown in Figure 1. The linear moving accuracy of the table was about 1 μm, and a uniform velocity was obtained. Scanning electron microscopy (SEM) and optical microscopy were used to observe the striation patterns.

IV. RESULTS AND DISCUSSIONS

A. *Temperature Distribution Map in the Specimen by FDM Simulation*

When a pulsed Nd:YAG laser beam was irradiated on the specimen tube, the calculated transient temperature profile along the circumferential direction from the irradiated region decreased. As an example, Fig. 5 shows the temperature distributions along the scanning direction and the circumferential direction when the power was 3.9 W, the pulse duration

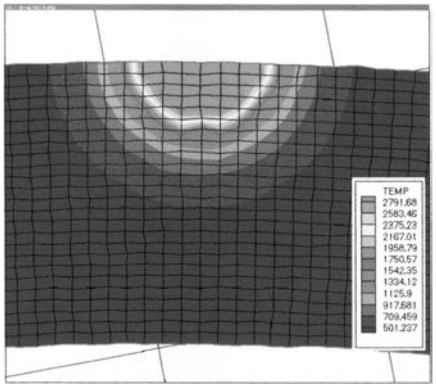

(*a*)

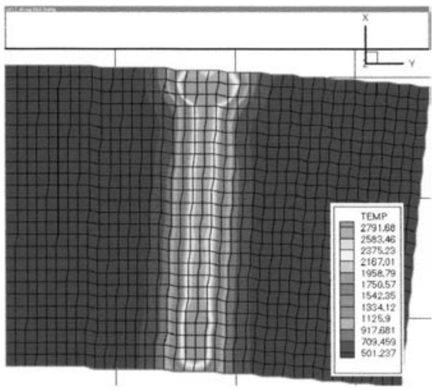

(*b*)

Fig. 6—Simulated temperature distributions in the cross section of the tube. Each mesh size was 5 μm: (*a*) when the melt ejection effect was not considered (2.7 W, 600 Hz, 0.12 ms, and 300 mm/min); and (*b*) when the melt ejection was considered above 2000 K (2.7 W, 600 Hz, 0.12 ms, and 300 mm/min).

was 0.12 ms, the frequency was 600 Hz, and the scanning speed was 300 mm/min. Figure 5(a) shows the temperature distribution on the surface of the specimen, and each mesh size was 5 μm. Figures 5(b) and (c) show the temperature distributions in the center of the thickness and the bottom of the specimen. As shown in these figures, striation patterns were clearly revealed. Of course, the temperature profiles would vary depending upon the laser power and pulse duration. The temperature near the molten region would decrease rapidly due to conduction cooling and the melt ejection effect. When the irradiated region was not melted, the temperature would decrease primarily due to conduction cooling. However, if the melting occurred during laser irradiation, the main heat loss mechanism was attributed to the melt ejection effect. Numerous workers have calculated the temperature profiles during laser irradiation by computer simulation. However, it was difficult to develop an investigation to predict the striation formation by application of simulation results and to analyze the relationship between striation formation and temperature distribution in a laser cutting process. Therefore, in order to explain the formation of the striation pattern on a cut edge, a maximum temperature profile map during the cutting process was applied.

Figure 6 shows two different models of simulated temperature distribution in the cross section of a thin STS 316L stainless steel tube during laser irradiation by considering the melt ejection effect. If melt ejection did not occur in the specimen even above the melting point of the metal, the major heat loss mechanism was by a conduction process and the simulated temperature distribution is shown in Figure 6(a). Meanwhile, if the melt ejection was assumed to occur in the specimen above 2000 K, the main heat loss mechanisms were by conduction and the melt ejection effect, and the temperature distribution is shown in Figure 6(b). If melt ejection was not considered, full penetration cutting was not achieved in the simulated work, as shown in Figure 6(a). Experimental results of laser cutting revealed similar phenomena. In laser cutting of specimens in this experiment, full penetration cutting was not possible without gas flow under almost all laser irradiation conditions, where melt ejection did not occur, because the gas flow enhanced the ejection of molten metal. The energy density was not sufficiently high for keyhole formation and to achieve full penetration only by evaporation. Although the melt ejection effect was affected by gas pressure and flow rate during the cutting, the experiment had been conducted at 4 atm, because the melt ejection was almost insensitive to gas pressures above 3 atm. Even if full penetration was obtained in a specimen by the melt ejection effect, the shape of the cut wall was quite different depending upon the laser energy density, pulse duration and scanning speed, *etc.* The combinations of these variables were very important for the formation of striation patterns in the cut walls and melt pool behavior.

Figure 7 shows three different models of temperature distribution profile in a cross section obtained by FDM simulation for different combination of variables. Figure 7(a) shows the temperature distribution in cross section of the specimen when the energy density was high enough to provide full penetration by melt ejection and the combination of laser variables satisfied the form of full penetration. The melt pool in the top region was formed in a semicircular shape and the entire region resembled the keyhole type. This shape of the melt pool is frequently seen in a keyhole-type welding process. The reason was probably due to low laser beam absorbance and fast conduction of heat in the initial laser irradiation period. However, once the top surface was heated above the melting point, the laser beam absorbance increased, as shown in Figure 2, and the oxidation heat was added to the molten metal. The temperature of the irradiated region would then be increased dramatically, and the melt ejection would take place under certain conditions. If the melt ejection did not take place in the upper region, the cutting front would not penetrate into the depth, as in Figure 6(a), because the laser energy was not sufficient to evaporate the entire volume of the cut region. If the upper region was emptied by the melt ejection effect, the laser beam would penetrate into the inner region. The temperature in this region would then be increased, and then melt ejection would occur again. The sequential repetitions of melt ejection and heating beneath the molten region would be continued during the laser irradiation. Therefore, the cross section of the cut region would retain a narrow cutting width.

The temperature distribution in the cross section can be changed depending upon the different combinations of pulse width and scanning speed, as mentioned earlier. Figure 7(b) shows the simulated temperature distribution in the cross section of the specimen when the combination of variables did not satisfy formation of full penetration of the tube thickness. The pulse duration was short; therefore, it was

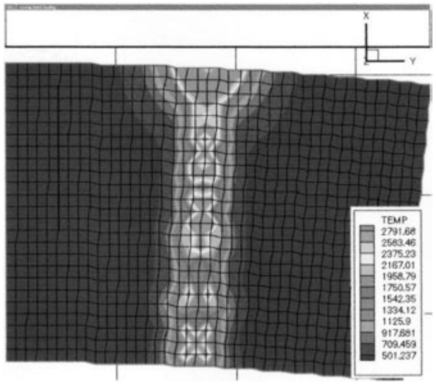

(*a*)

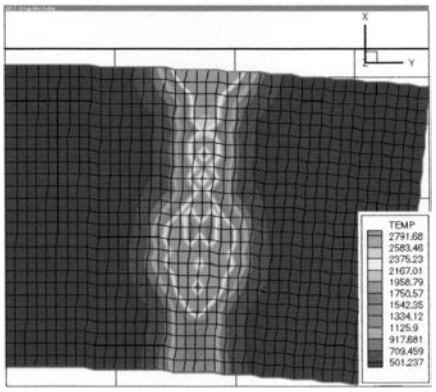

(*b*)

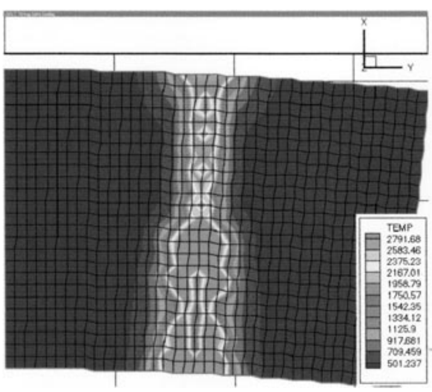

(*c*)

Fig. 7—Simulated temperature distributions in cross section. (*a*) When the laser energy density was high enough to cause full penetration by the melt ejection effect (3 W, 0.12 ms, 600 Hz, and 300 mm/min). (*b*) When the combinations of variables did not satisfy formation of full penetration of tube thickness by one pulse (2.7 W, 0.12 ms, 600 Hz, and 300 mm/min). (*c*) When melt ejection did not take place in the lower part of tube (2.7 W, 0.12 ms, 800 Hz, and 300 mm/min).

assumed that the laser pulse was irradiated in the middle of the cross section before full penetration was achieved in the specimen by previous pulse. The simulated temperature showed that the maximum temperature was obtained at the central region of the cross section. If full penetration did not occur through the entire thickness of the specimen within a pulse duration before the next pulse was irradiated on the adjacent area of the surface, striation patterns on the cut wall would be irregular shapes due to lack of a smooth temperature distribution, as shown in Figure 7(b). Sometimes full penetration cutting was not achieved in the case of a short pulse duration and high scanning speed even with high energy density.

Figure 7(c) shows the simulated temperature distribution in a cross section of the specimen when the energy density was relatively low, although the combinations of variables satisfied formation of full penetration. The lower region revealed a relatively high temperature because the energy density was not high enough to cause much ejection of molten metal. Although melt ejection might occur in the upper region, this would not maintain the sequence of melting and ejection below the middle region. The energy loss due to melt ejection would then be reduced, and the accumulated energy would increase the temperature in the lower molten region. Also, the conduction of heat would be hindered by the decreased thermal conductivity of metal there. Therefore, the volume of molten metal would increase temporally in the lower region, as shown in Figure 7(c), and it would be ejected by the gas flow.

B. *Effect of Variables in Striation Formation on Cut Wall*

The laser power, pulse duration, frequency, and scanning speed are very important in the formation of striation patterns on cut walls. The relationship between temperature distributions and striation patterns was obtained depending upon the combinations of the preceding variables and also the changes in each variable. In order to compare the simulated results with real striation patterns on a cut wall, experiments were carried out to obtain the real striation patterns under the same laser irradiation conditions that were used to simulate the patterns.

Figure 8 shows the simulated temperature distributions and experimental striation patterns as a function of pulse duration at the same laser power, frequency, and scanning speed. The striation patterns were clearly revealed in the case of a long pulse duration, as shown in Figure 8(c). It is believed that the pulse duration was sufficient for full penetration and to cut the entire thickness at this scanning speed. Therefore, it was possible for a long pulse to remove more molten metal from the cutting front. The striation patterns were fairly regular, and the width of the striation was almost constant. According to the simulated temperature distribution, high-temperature spots were observed in the middle of the cross-sectional area. A hot spot might originate for several reasons. The simulation had been performed under the condition of the occurrence of melt ejection. If the central region did not satisfy the melt ejection condition, the heat loss due to melt ejection would not take place, and the calculated temperature would reach quite high values. Hot spots would then appear on the central region. Another possible reason might be that it was difficult for the early melt ejection to occur, because the absorbed energy during the early laser pulse was relatively lower than that of the later part due to lower absorbance at lower temperature at the surface. If another pulse were irradiated again on the melted region, as described in Figure 7(b), then the hot spot would occur. If a melt ejection did not occur, the regular striation patterns might not be formed regardless of pulse duration. However, if melt ejection could take place, the shape of the striation patterns would be affected by the hot spot region. The striation patterns seemed to be clearly

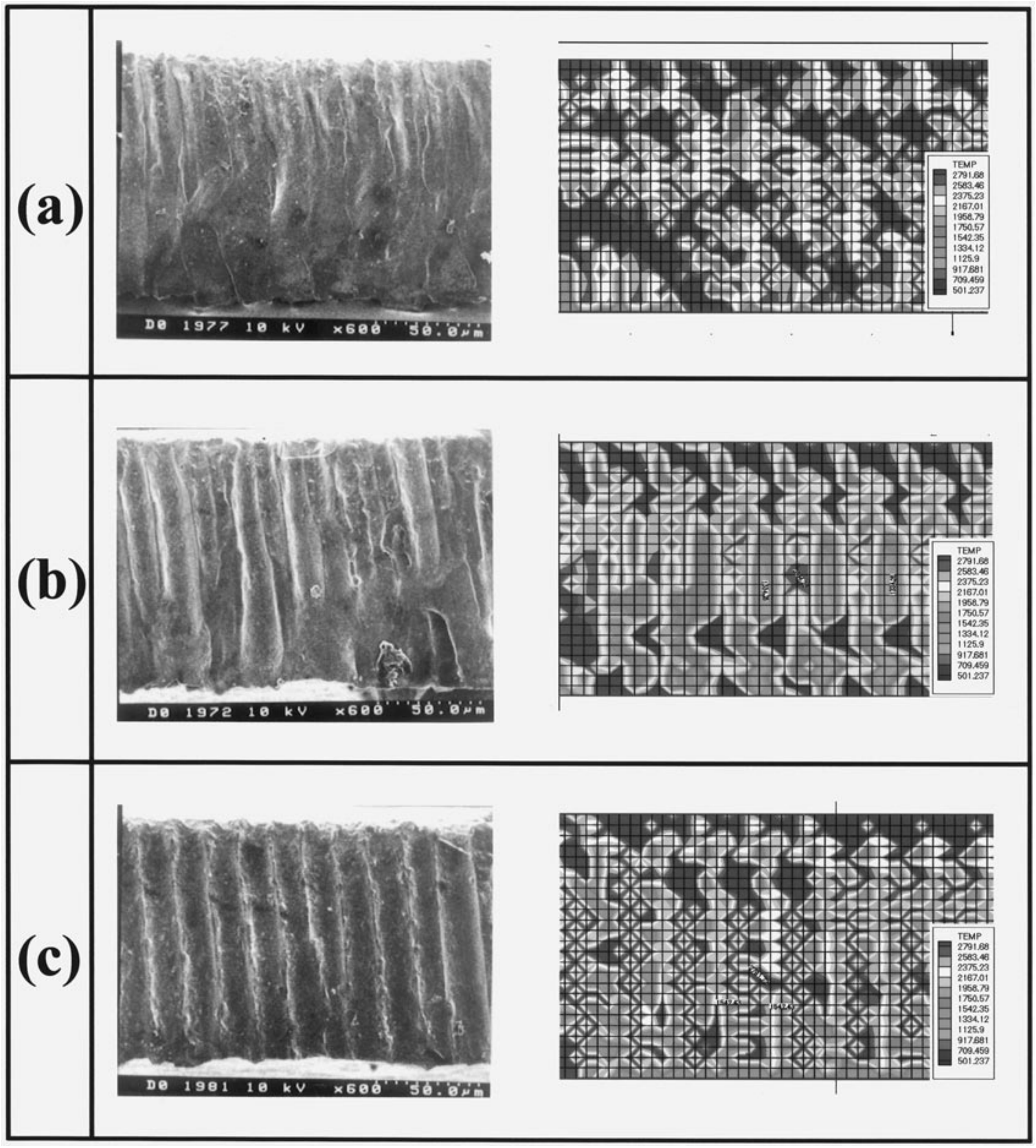

Fig. 8—Striation patterns on cut walls obtained by laser irradiation and simulation of different pulse duration: (*a*) 0.12 ms (2.7 W, 600 Hz, and 300 mm/min), (*b*) 0.14 ms (2.7 W, 600 Hz, and 300 mm/min), and (*c*) 0.18 ms (2.7 W, 600 Hz, and 300 mm/min).

shown when the hot spot area was reduced. Sometimes full penetration cutting was not performed well under 0.12 ms pulse duration in spite of the same conditions except for the pulse duration. Figure 8(a) shows almost a flat surface, which was desirable in laser cutting.

Figure 9 shows the simulated temperature distributions and experimental striation patterns as a function of scanning speed at the same laser power, frequency, and pulse duration. Although the striation patterns were quite irregular in the experimental results, as shown in Figure 9(a), regular hot spots were revealed in the simulated result. The hot spots were regarded as melt ejection areas, and also there were areas where the laser beam was irradiated. Therefore, those regions have a higher temperature than other melted regions. The scanning speed was lower in Figure 9(a) than in the other cases of Figures 9(b) and (c); therefore, the energy density would be much larger in this case. As the scanning speed had increased, the energy density decreased and hot spots disappeared, as shown in the simulated results. At a scanning speed of 500 and 800 mm/min, hot spots were not obtained in the simulated temperature distribution and those results corresponded well with the striation patterns in the SEM photographs in Figures 9(b) and (c). According to the experimental results, the tendency of dross attachment had increased at high scanning speed, *i.e.*, low energy density. However, it was difficult to predict the dross attachment from the simulation results. The dross attachment is caused by low viscosity of the molten metal on the bottom. Under low energy density condition, ejection did not easily occur due to a lower melt temperature, and, thus, the molten metal solidified at the bottom before the ejection had taken place due to the high scanning speed.

Figure 10 shows the simulated temperature distributions and experimental striation patterns as a function of power level at the same scanning speed, pulse duration, and frequency. The simulated results revealed well-defined striation

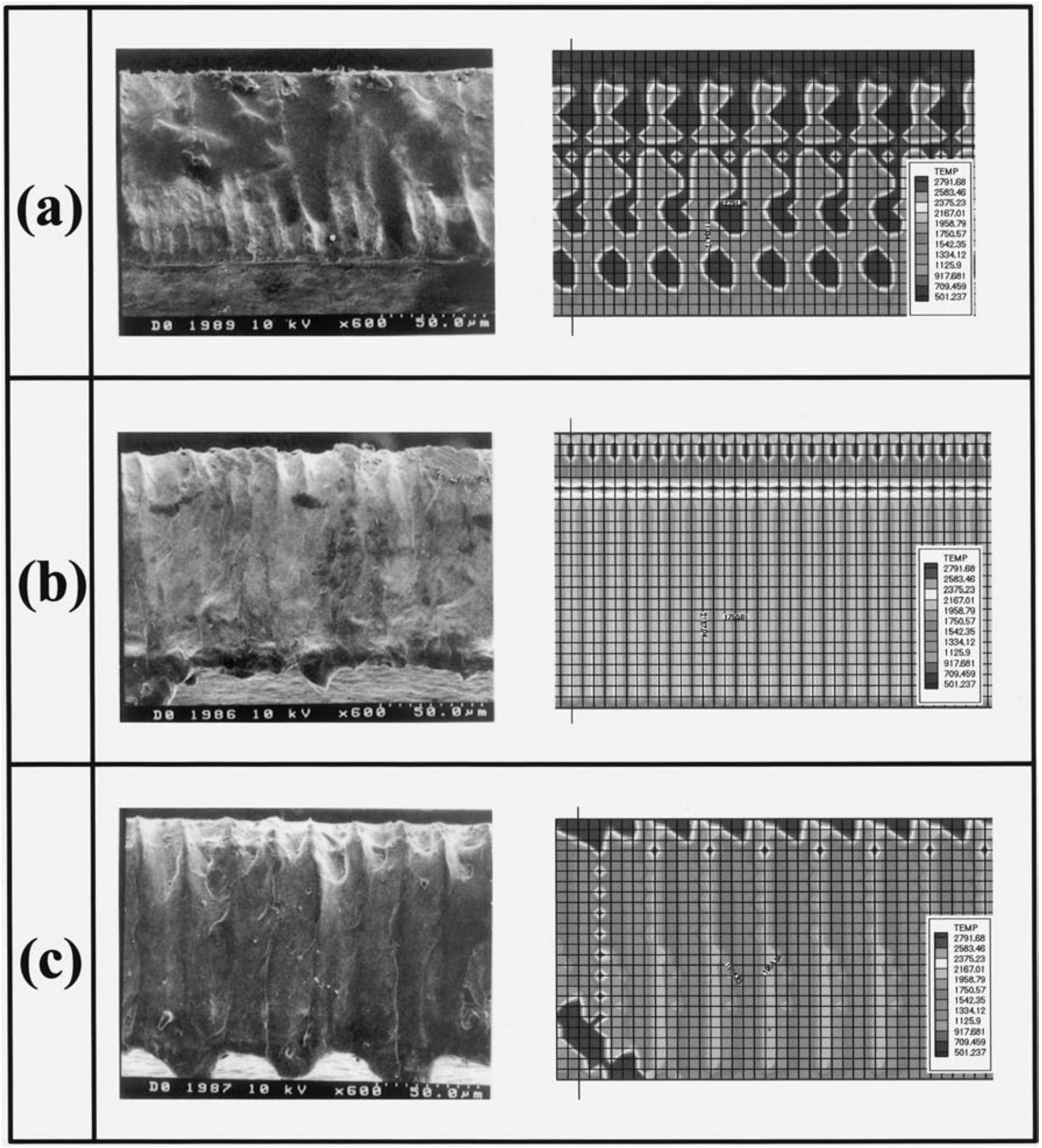

Fig. 9—Striation patterns on cut walls obtained by laser irradiation and simulation of different scanning speeds: (*a*) 100 mm/min (2.7 W, 600 Hz, and 0.12 ms), (*b*) 500 mm/min (2.7 W, 600 Hz, and 0.12 ms), and (*c*) 800 mm/min (2.7 W, 600 Hz, and 0.12 ms).

patterns at a certain power level, whose shapes corresponded well with the experimental results, as shown in Figure 10(b). As the laser power had been increased to 5 W, as shown in Figure 10(c), the simulated temperature increased to high values, as expected.

Figure 11 shows the simulated temperature distributions and experimental striation patterns as a function of pulse frequency at the same power level, scanning speed, and pulse duration. The simulated results and experimental results revealed unclear and complex striation patterns at 600 Hz, as shown in Figure 11(a).

In the formation of striation patterns, the laser power density was revealed as the most important factor, since the laser power density is most influential in the heating of metal, and the striation formation is caused by the ejection of molten metal and evaporation during laser cutting process. The power density of the laser beam was related to variables such as laser power, pulse duration, frequency, and scanning speed. However, the simulation results revealed that melt ejection and hot spots were important to the formation and the shape of the striation patterns.

The narrow kerf width is very desirable for laser cutting of materials, especially for corner cutting and complex shape cutting. Although the kerf width changed depending upon the depth profile, it was strongly affected by the laser parameters. Usually, the minimum kerf width was achieved by a small spot size and a high laser energy density for thin metal. It is known that the striation formation on a cut wall by a continuous laser beam is caused by molten metal fluctuation, which is related to heat transfer, chemical reaction and hydrodynamic instability, *etc.* The laser cutting by a pulsed beam involves more complicated phenomena than that by a continuous beam,

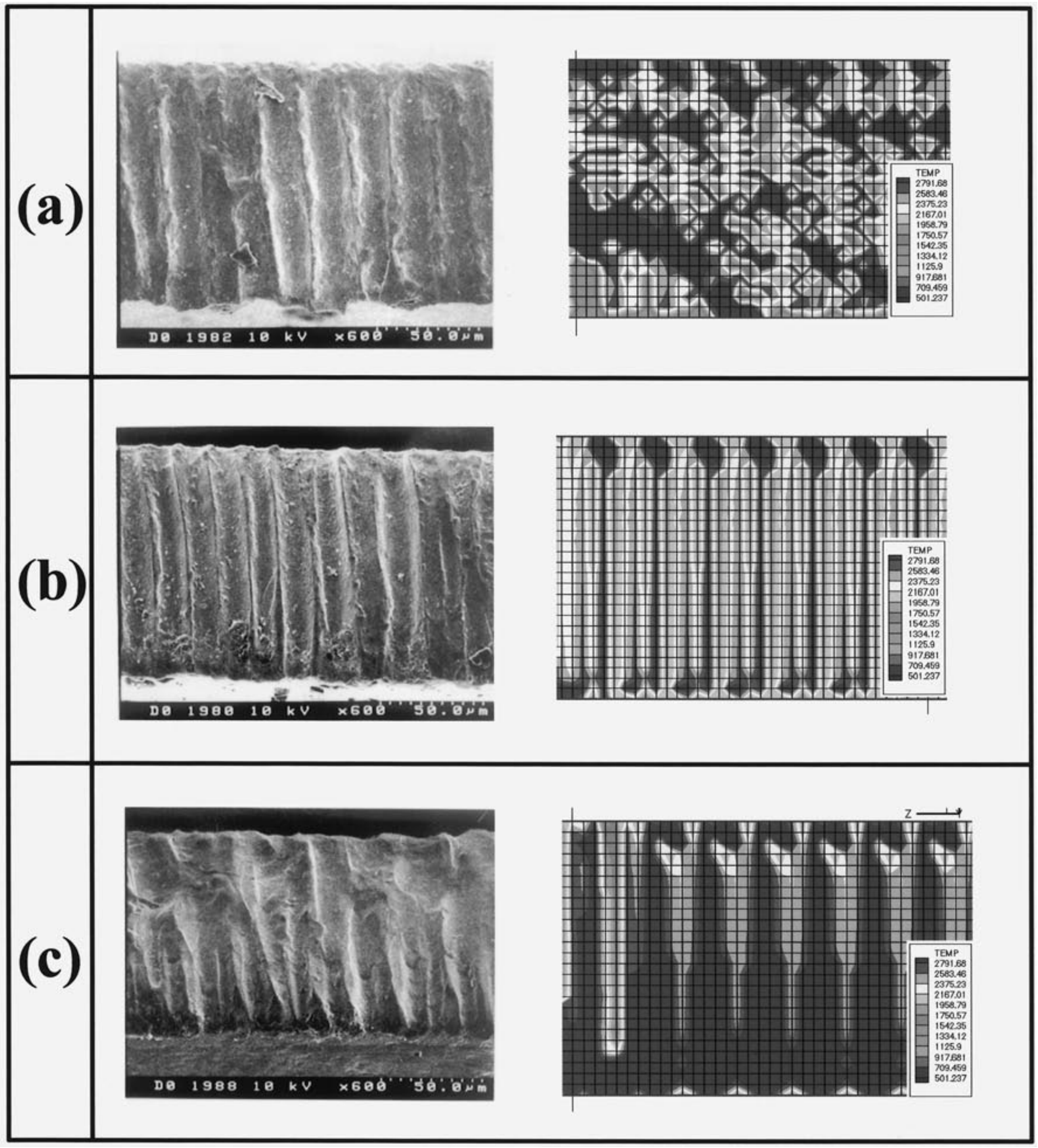

Fig. 10—Striation patterns on cut walls obtained by laser irradiation and simulation of different powers: (*a*) 3 W (300 mm/min, 0.12 ms, and 600 Hz), (*b*) 3.9 W (300 mm/min, 0.12 ms, and 600 Hz), and (*c*) 5 W (300 mm/min, 0.12 ms, and 600 Hz).

and the simulation did not fully consider a detailed real situation. Nevertheless, this simulation method offered a good tool for analysis of complex striation formation in pulsed laser beam cutting. Therefore, the numerical simulation can predict the shape of striation patterns and render a flat cut wall by selection of optimized laser parameters.

V. CONCLUSIONS

In the cutting of a thin stainless steel tube by a pulsed Nd:YAG laser beam, a numerical simulation method was developed using a moving pulsed heat source and melt ejection phenomena, and the quantitative effects of laser processing parameters were determined in temperature distribution diagrams. The temperature distribution obtained by numerical simulation can be applied to predict the shape of striation patterns during the laser cutting process.

Although the shape of the striation pattern was influenced by different combinations of laser parameters such as laser power, pulse duration, frequency, and scanning speed, the laser power density was revealed as the most important factor in the formation of striation patterns, since the laser power density is the most influential factor in the heating of metal, and the striation formation is caused by the ejection of molten metal and evaporation during laser cutting process. Although high energy density had resulted in clear regular striation patterns, relatively low energy density caused the formation of a hot spot, which hindered the formation of regular striation and provided irregular patterns. The simulated results showed good agreement with the experimental

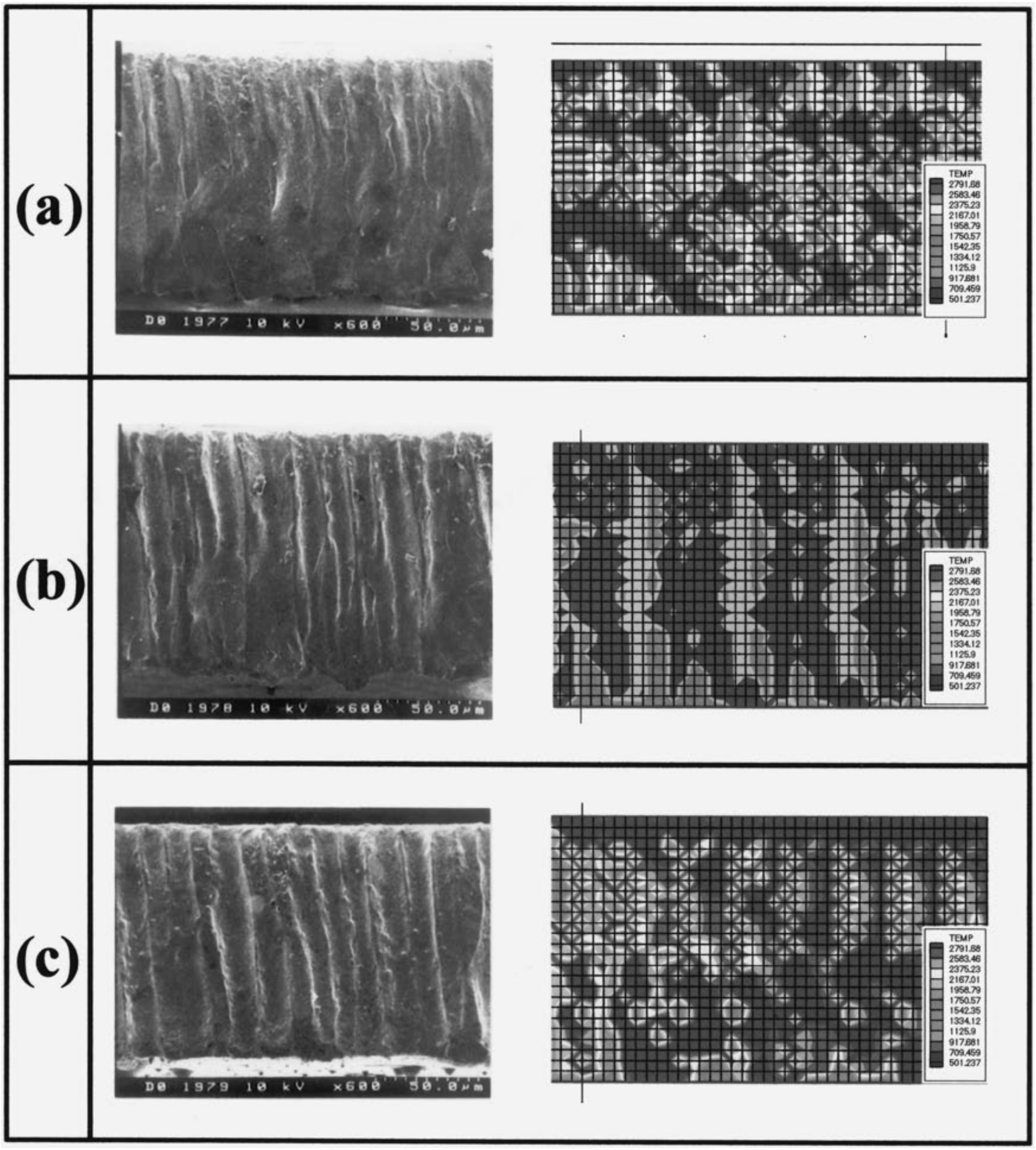

Fig. 11—Striation patterns on cut walls obtained by laser irradiation and simulation of different frequencies: (*a*) 600 Hz (2.7 W, 300 mm/min, 0.12 ms), (*b*) 700 Hz (2.7 W, 300 mm/min, 0.12 ms), and (*c*) 800 Hz (2.7 W, 300 mm/min, 0.12 ms).

results. The simulated results could predict the shape of striation patterns and offered a way to provide flat cut walls.

REFERENCES

1. J.D. Chung, J.S. Lee, K.H. Whang, and T.H. Kim: *J. Mater. Processing Manufacturing Sci.*, 1996, vol. 5 (1), pp. 3-15.
2. K.A. Bunting and G. Cornfield: *J. Heat Transfer*, 1975, vol. 97, pp. 116-22
3. W.W. Duley: *CO_2 Laser*, Academic Press, New York, NY, 1976, pp. 248-63.
4. Y. Arata, H. Maruo, I. Miyamoto, and S. Takeuchi: *Trans. JWRI*, 1979, vol. 8 (2), pp. 15-26.
5. A. Ivarson, J. Powell, J. Kamalu, and C. Magnusson: *J. Mater. Processing Technol.*, 1994, vol. 40, pp. 359-74.
6. John Powell: *CO_2 Laser Cutting*, Springer-Verlag, New York, NY, 1998, pp. 214-15.
7. J. Mazumder and W.M. Steen: *J. Appl. Phys.*, 1980, vol. 51 (2), pp. 941-47.
8. T.H. Kim, K.C. Chong, B.Y. Yoo, J.S. Lee, and K.H. Whang: *J. Mater. Sci.*, 1995, vol. 30 (3), pp. 784-92.
9. C.P. Hong and W.H. Baek: *J. Kor. Inst. Met.*, 1998, vol. 26 (8) pp. 810-21.
10. Y. Bayazitoglu and M.N. Ozisik: *Elements of Heat Transfer.* McGraw-Hill, New York, NY, 1988, pp. 209-14.